# The lizard genera *Bainguis* and *Parmeosaurus* from the Upper Cretaceous of China and Mongolia

1,2,3*Liping Dong, 1,2Xing Xu, 1,2Yuan Wang, 4Susan E. Evans

1 *Institute of Vertebrate Paleontology and Paleoanthropology, Chinese Academy of Sciences, 142 Xi-Zhi-Men-Wai St, P.O. Box 643, Beijing 100044, China*

2 *Key Laboratory of Vertebrate Evolution and Human Origin, Chinese Academy of Sciences, 142 Xi-Zhi-Men-Wai St, P.O. Box 643, Beijing 100044, China*

3 *State Key Laboratory of Palaeobiology and Stratigraphy (Nanjing Institute of Geology and Palaeontology, Chinese Academy of Sciences), 39 East Beijing Road ,Nanjing 210008, China*

4 *Department of Cell and Developmental Biology, University College London, Gower Street, London, WC1E 6BT, UK*

*corresponding author: dongliping@ivpp.ac.cn

**Abstract**

The lizard genus *Bainguis* was originally described from the Upper Cretaceous of Mongolia and attributed to Anguimorpha. The same genus was later reported from the Upper Cretaceous of Bayan Mandahu, Nei Mongol, China on the basis of a partial skeleton showing some similarities in osteoderm morphology. Re-examination of this specimen with the aid of μCT scanning suggests that it is, in fact, attributable to *Parmeosaurus*, a scincoid lizard described from the Ukhaa Tolgod locality, Mongolia, as do two new specimens from Bayan Mandahu. Moreover, some of the Mongolian material originally attributed to *Bainguis* appears also to belong to *Parmeosaurus*. And our new phylogenetic analysis confirms that *Parmeosaurus* is positioned on the stem of Scincoidea. Taken together, these specimens add new data to our understanding of *Parmeosaurus* but also raise questions as to the affinities of *Bainguis*.

Keywords: *Parmeosaurus*, *Bainguis*, Late Cretaceous, Gobi desert, China, Taxonomy

## Introduction

In 1984, Borsuk-Białynicka described several new lizard taxa from the Upper Cretaceous locality of Bayn Dzak, Mongolia, and attributed them to Anguimorpha. One of these, interpreted as a stem-anguimorph ('pre-anguimorph grade'), was *Bainguis parvus.* The designated holotype skull (Institute of Paleobiology, Polish Academy of Sciences, Warsaw, ZPAL MgR-II/46) has osteodermal encrustation on the cranial bones and rectangular osteoderms covering the dorsum of the neck. A second, juvenile, skull (ZPAL MgR-II/90) was referred to the same species on the basis of proportional similarities with the holotype. In addition, Borsuk-Białynicka attributed three postcranial fragments (ZPAL MgR-II/9, II/10, II/11) to *Bainguis* based on osteoderm shape. These postcranial fragments were not described in the journal article, but vertebrae and osteoderms from ZPAL MgR-II/11 were figured (Borsuk-Białynicka, 1984: plates 2:1e and 13:5, respectively [but note that the figure caption on p.99 denoted the first of these as 2:2]). In 1996, Gao and Hou described new lizard material from the Chinese Nei Mongol locality of Bayan Mandahu (Upper Cretaceous, Campanian). Among these specimens was an incomplete postcranial skeleton (Institute of Vertebrate Paleontology and Paleoanthropology, Beijing, IVPP V 10080) enclosed in rectangular, imbricate osteoderms, but with parts of the axial skeleton, pectoral and pelvic girdles, and limbs exposed. On the basis of the rectangular osteoderms, Gao and Hou referred the skeleton to *Bainguis* and, therefore, to Anguimorpha. In 2000, Gao and Norell described a new Late Cretaceous (Campanian) lizard from the Ukhaa Tolgod locality, Mongolia, under the name *Parmeosaurus scutatus* (holotype, Institute of Geology, Mongolian Academy of Sciences, Ulaanbaatar, IGM 3/138). *Parmeosaurus* also had rectangular osteoderms, with those of the dorsum being described as twice the width of those on the venter. Gao and Norell referred *Parmeosaurus* to the Scincoidea, a position supported by the analyses of Gauthier et al. (2012), Reeder et al. (2015), and Pyron (2017), although Conrad (2008) placed it in a more stemward position.

Two different lizard taxa, with similar rectangular osteoderms, have therefore been described from the Campanian of Mongolia and Chinese Nei Mongol: a putative stem-anguimorph, *Bainguis*, and a stem-scincoid, *Parmeosaurus*. This raises the possibility of misattribution if incomplete specimens are identified on the basis of osteoderm shape. Herein, we re-describe

IVPP V 10080, incorporating new μCT scan data, and reassess its attribution to *Bainguis.* We also describe two new osteoderm-bearing specimens from Bayan Mandahu.

**Abbreviations**

acet, acetabulum; add.fs, adductor fossa; aip, anterior inferior process of prootic; am.pr, anteromedial process (of coronoid); an, angular; an.ft, angular facet; an.pr, anterior process (of interclavicle); ar.pro, alar process of prootic; a.san.f, anterior surangular foramen; asca, astragalocalcaneum; a.vc, anterior opening of vidian canal; bo.co, basioccipital condyle; bpt, basipterygoid process; b.tb, basal tubercle; cla, clavicle; co, coronoid; ch.ty.n, chorda tympani nerve opening; cr.pro, crista prootica; cr.se, crista sellaris; den.ft, dentary facet; ds.pr, dorsal process (of coronoid); dt3, distal tarsal 3; dt4, distal tarsal 4; ecpt, ectopterygoid; ept, epipterygoid; fem, femur; fib, fibula; f.6, foramen for abducens nerve; f.7, foramen for facial nerve; f.12, foramen for hypoglossal nerves; f.ed, foramen for the endolymphatic duct; fs.c, fossa columellae; f.vb, fenestra vestibuli; hsc, horizontal semicircular canal; hum, humerus; icf, internal carotid foramen; icla, interclavicle; icond.gv, intercondylar groove; il, ilium; isc, ischium; isc.tb, ischial tubercle; ju, jugal; L, left; la.pr, lateral process (of astragalocalcaneum); lrst, lateral opening of recessus scalae tympani; man.co, mandibular condyle; md.cr, median crest (of supraoocipital); mrst, medial opening of recessus scalae tympani; mt, metatarsal; mt5, metatarsal V; obtu.f, obturator foramen; oc.r, occipital recess; osd, osteoderm; pa, parietal; pacet.pr, preacetabular process; pa.f, parietal foramen; p.as, processus ascendens; p.av, posterior opening of vidian canal; p.co, primary coracoid emargination; pect.tb, pectineal tubercle; pm.pr, posteromedial process (of coronoid); pob, postorbital; pocc, paroccipital process; psp, parasphenoid; pt, pterygoid; pub, pubis; pub.l.pr, pubic lateral process; p.san.f, posterior surangular foramen; qu, quadrate; R, right; rad, radius; rap, retroarticular process; san+ar, surangular+articular; sa.v, sacral vertebrae; scco, scapulocoracoid; scco.f, scapulocoracoid foramen; spl.ft, splenial facet; sq, squamosal; st, supratemporal; stg.pr, supratrigeminal process; st.pr, supratemporal process (of parietal); tib, tibia; tr.v, trunk vertebrae; ty.cr, tympanic crest

**Material and Methods**

Bayan Mandahu (Fig.1) is one of several Upper Cretaceous localities in the Gobi Basin of China, and Mongolia that have yielded lizards, including the enigmatic burrowing *Sineoamphisbaena* (Wu et al., 1996). The fossiliferous beds at Bayan Mandahu are referred to the Djadochta Formation which is considered to be Campanian in age (~75 Ma, Jerzykiewicz et al., 1993), although there are debates as to the correlation between the Mongolian Djadochta fossil-bearing beds and the Bayan Mandahu beds. Some researchers have argued that the beds at Bayan Mandahu are equivalent to the lowest Upper Cretaceous red beds exposed in the Gobi area of the Mongolian Plateau (i.e., Bayan Mandahu fossiliferous beds are lower than those in Mongolia) based on the faunal composition (Makovicky, 2008; Xu et al., 2013). The environment has been reconstructed as arid or semi-arid (Eberth, 1993), and the locality has yielded turtles (e.g. Brinkman and Peng, 1996), dinosaurs (e.g. You and Dong, 2003; Pittman et al., 2015), dinosaur eggs (Dong and Currie, 1996), and mammals (Ladevèze et al., 2010; Meng, 2014), as well as lizards (Gao and Hou, 1996). The lizard fauna shows similarities to that from the Mongolian Gobi Basin, with the genera *Priscagama*, *Mimeosaurus*, *Adamisaurus* and *Carusia* present at both localities (Gao and Hou, 1996; Gao and Norell, 2000). However, three genera, *Xihaina*, *Anchaurosaurus*, and *Sinoamphisbaena* (Gao and Hou, 1995, Wu et al., 1993) are known only from Bayan Mandahu, whereas some common lizards from the Mongolian Gobi Basin, such as *Slavoia* (Tałanda, 2016) are unrecorded from Bayan Mandahu.

IVPP V 10080 (Fig. 2) is the postcranial skeleton (including the integument) of a medium-sized lizard, in which the pectoral girdles and part of a humerus have been prepared free from the rest of the skeleton which is covered by osteoderms. More recent (2012) fieldwork at Bayan Mandahu yielded two small blocks (IVPP V 23897, V 23898) (both under the same field number 12WL-7) from the site of E106°44′45.9″, N41°44′18.5″. Both specimens bear osteoderms identical to those on IVPP V 10080. One contains postcranial material and the other a partial skull. The blocks were found together (under the same field number), are of similar size, and have non-overlapping elements. They are therefore probably, but not irrefutably, from the same individual. Separate catalogue numbers were given to the blocks, to be cautious.

IVPP V 10080 and IVPP V 23897 (Fig. 3) were scanned at the Key Laboratory of Vertebrate Evolution and Human Origins, Chinese Academy of Sciences (CAS) at IVPP, using 225 kV micro-computerized tomography (developed by the Institute of High Energy Physics, CAS, Beijing) with a Phoenix X-ray source. IVPP V 10080 was scanned along the longitudinal axis of the specimen twice successively with a beam energy of 130 kV and a flux of 120 uA at a detector resolution of 53.30 um per pixel using a 360° rotation with a step size of 0.5° and an unfiltered aluminium reflection target, whereas the specimen IVPP V 23897 was scanned with a beam energy of 110 kV and a flux of 170 uA at a detector resolution of 16.50 um per pixel. A total of 720 transmission images were reconstructed for each scan in a 2048 x 2048 matrix of 1536 slices using a two-dimensional reconstruction software developed by the Institute of High Energy Physics, CAS. Surface models were rendered using VG Studio 2.1 and Mimics Research 18.0.

One of us (LD) also re-examined the type and referred material of *Bainguis* at the Institute of Paleobiology, Warsaw, Poland. A scanned skull of *Parmeosaurus scutatus* (IGM 3/139) (The Deep Scaly Project, 2009) was referenced for comparison and phylogenetic analysis.

**Systematic Palaeontology**

Squamata Oppel, 1811

"stem Scincoidea" Gauthier et al., 2012

*Parmeosaurus scutatus* Gao et Norell, 2000

1996 *Bainguis* sp., cf. *B. parvus* Gao et Hou, p. 589, Fig. 6

2000 *Parmeosaurus scutatus* Gao et Norell, p. 74, Fig. 24, 25

Holotype: IGM 3/138, well-preserved skull with articulated postcranial skeleton (Gao and Norell, 2000).

Type locality and horizon: Ukhaa Tolgod, Mongolia; Upper Cretaceous Djadochta Formation.

New material: IVPP V 10080, articulated postcranial skeleton enclosed by osteoderms (Gao and Hou, 1996, referred by them to *Bainguis*); IVPP V 23897, partial skull with a few dorsal

osteoderms; IVPP V 23898, humerus, with some ventral osteoderms. All new material is from the Bayan Mandahu locality, Nei Mongol, China, which is Campanian in age.

Distribution: Ukhaa Tolgod, Mongolia; Bayan Mandahu, China; Djadochta Formation (Campanian)

Differential diagnosis (revised from Gao and Norell, 2000): Small to medium-sized lizard resembling scincoids (members of Scincoidea sensu Gauthier et al., 2012) in the combination of the following characteristics: dorsal and ventral osteoderms present, with ventral elements compound (duplex); cephalic osteoderms present; palpebral ossification present; small lateral coronoid process of the dentary extending on to anterolateral surface of coronoid; retroarticular process inflected medially with small flange on medial margin; subdental ridge of the dentary well-developed; marginal teeth fully pleurodont and densely spaced. Differs from other scincoid taxa in having a narrow elongate skull with a laterally compressed rostrum; parietal table with well-developed lateral flange for dorsal origin of adductor musculature; marginal teeth robust with tricuspid crowns; autotomy fracture plane positioned posterior to caudal transverse processes.

**IVPP V 10080**

The specimen comprises a partially prepared postcranial skeleton of a medium-sized lizard. The skull and neck are missing and much of the internal skeleton is obscured by the overlying body armour, but the pectoral girdles and part of a humerus have been prepared free from the rest of the skeleton, and some osteoderms were removed to reveal the pelvic girdles and parts of the limbs. The µCT scan has revealed additional details of the dorsal, sacral and caudal vertebral column and ribs, as well as of the limbs and their girdles. The description below is based primarily on the µCT data, supplemented with details observed directly from the specimen.

*Axial skeleton*: The µCT scan (Fig. 4) revealed an articulated series of 13 dorsal, 2 sacral and 12 anterior caudal vertebrae. Based on the position of the pectoral girdle, we estimate there would have been a minimum of five further dorsal vertebrae. Assuming a typical cervical

count of 7–8 cervicals, this would give an estimated presacral count of 25–26. The vertebrae are procoelous, with roughly triangular centra, rounded condyles, and no precondylar constriction. The second dorsal centrum preserved has a length of 3.71 mm and an anterior width of 4.5 mm, and the other dorsals are of similar proportions. The neural spines are rectangular, posteriorly placed on the neural arch, and of medium elevation. Judging from the scan reconstructions, the vertebrae appear to possess weakly developed accessory articulations. The dorsal ribs are long and slender, but it is not clear whether free ribs were present on the last dorsal vertebrae. The two sacral vertebrae have short centra and robust sacral ribs, the first being expanded mainly in the dorso-ventral plane and the second in the horizontal plane. Together they form a somewhat triangular surface that is apposed to the medial side of the iliac blade. The first four anterior caudal vertebrae have unusually long, slender transverse processes (central length 3.0–3.4 mm; width from mid-point of centrum to tip of transverse process, 6.9 mm). These anterior caudals are followed by five vertebrae of gradually increasing central length and decreasing width, and then by a further series of vertebrae with longer centra and little or no transverse processes (preservation precludes measurement). The μCT scans have also confirmed the presence of an autotomy septum lying behind the caudal rib and starting at the ninth caudal vertebrae (Fig. 4; Supplementary Video). Haemal arches are present from the second caudal as there is clearly a pair of pedicles present at the distal end of each centrum for the attachment of the haemal arch. The pedicles lie immediately anterior to the condyle so that the haemal arches were almost intercentral in position. Several haemal arches are preserved in the tail region, but are separated from the vertebrae. The arches are Y-shaped distally but one more proximal element preserves the intercentral bar. The two haemals more distally on the tail lack the cross-bar.

In the area of the ischiopubic (thyroid) fenestra a long tapering element is preserved that looks like a displaced posterior trunk rib. Two similar elements lie further distally below the second and third caudals, and below the tenth caudal vertebra respectively.

*Pectoral girdle and forelimb.* The pectoral girdle (Fig. 2) was on a small block that has been removed from the main block. The humerus was broken into two parts, with one part

208 remaining on the main block and thus allowing the small block to be positioned. The girdle
209 displays a gracile, cruciform interclavicle (Fig. 2C) with a well-developed anterior process and
210 long lateral processes that terminate in a small posteriorly directed hook. The anterior process
211 separates the clavicles in the midline. The ventral ends of the clavicles are expanded and
212 perforate, and the bones taper gradually toward their dorsal ends. The endochondral part of
213 the girdle is represented by a fully fused scapulocoracoid that preserves the glenoid cavity for
214 the humerus and, anterior to it, a scapulocoracoid foramen, and a primary coracoid
215 emargination. The proximal head of the left humerus is preserved in articulation with the
216 glenoid. It is well ossified but the proximal epiphysis appears to be separate, suggesting that
217 the animal may not have been fully mature, despite the fusion of the girdle elements. The
218 remainder of the humerus is on the main block. Its shaft is of medium length (reconstructed at
219 ~16.48 mm) and ends in a well-ossified distal head on which the condyles are fully ossified
220 (i.e. no separate epiphyses). No epipodials are in articulation with the humerus, but two
221 slender bones (10.6 mm) displaced posteriorly may be the radii.
222
223
224 *Pelvic girdle.* The pelvic girdle is nearly complete on both sides, except the posterior tip of the
225 ilium. The three elements, ilium, pubis, and ischium, are fully fused (there is no hint of suture
226 present on the µCT section images) (Fig. 4C). The ilium has a long gracile blade with a
227 tapering tip and a well-developed anterior preacetabular tuberosity for the ilio-pubic ligament
228 (Snyder, 1954). Medially, the sacral rib attachment lay a short distance posterodorsal to the
229 acetabulum, a position regarded by Borsuk-Białynicka (2007) as primitive for squamates. The
230 ischium and pubis enclose a large thyroid fenestra (Fig. 4A,B). The two pubes are angled
231 anteromedially. Each is relatively long and tapering, meeting in the ventral midline at a narrow
232 symphysis. A well-developed triangular processus lateralis pubis (sensu Russell and Bauer,
233 2008) is placed roughly half way along the margin of the bone. It extends into a distinct
234 incurved crest that runs along the medial margin of the pubis to its tip, thereby creating a
235 medial recess. The anteriormost extremity of the acetabulum bears the pectineal tubercle
236 anteriorly and in frontal of the tubercle is the obturator foramen. The ischium is roughly

237 trapezoidal, with a distinct but short posterodorsal angulation. The lamina is concave
238 ventrally.
239
240 *Hind limb.* Gao and Hou (1996) reported the left hind limb to be preserved in IVPP V 10080.
241 In fact, the limb they figured is the right, the left is represented only by the proximal end. The
242 epiphyses of the right femur are fully developed and, unlike those of the humerus, are fused
243 with the rest of the bone (Fig. 4C). Proximally, the femoral head is well-rounded and
244 separated from the internal trochanter by a deep intertrochanteric fossa. The bone is strongly
245 built, of medium length (20.8 mm, ~126% humerus), and sigmoid in shape. The distal end
246 displays a shallow intercondylar groove between the mesial and the slightly larger lateral
247 condyles. The tibia is also robust (14.6 mm, 70% of femoral length), and has a proximal head
248 that is triangular in cross-section. The fibula is equal in length to the tibia but is less than half
249 its diameter and there is a slight sigmoid twist to the shaft. The astragalus and calcaneum are
250 fully fused to form a proximodistally short but wide element in which the tibial and fibular
251 facets are well separated by a notch. Posteriorly, there is a lateral process. Distally, the
252 astragalocalcaneum has a large concave articular surface for an enlarged fourth distal tarsal
253 (DT4), which is preserved close to its original position. A hooked fifth metatarsal (MT5) is
254 preserved in articulation with DT4. It has a small outer process and well-developed lateral and
255 medial plantar tubercles. The shaft is short and slightly twisted. Distal to DT4 and MT5 are a
256 possible third distal tarsal, and the proximal heads of three other metatarsals. These
257 represent either MT1, 2, 3 or, more probably given their size, MT1, MT3 and MT4. Nothing is
258 preserved of the remainder of the foot.
259
260 *Osteoderms*: Osteoderms cover the whole body, including the limbs and tail. The dorsal
261 osteoderms (Fig. 2D) are rectangular and anteroposteriorly imbricate, with the glide surface
262 covering roughly one-third of the surface of each osteoderm. These osteoderms do not
263 overlap on their lateral borders, but appear rather to be loosely sutured along their margins.
264 There is a small amount of variation in the size of the dorsal osteoderms but most are 1.64–
265 1.79 mm in medio-lateral width and 2.58–2.89 mm in anteroposterior length. The ventral
266 osteoderms of the body and limbs, also with their anterior one-third as the glide surface, are

narrower (0.79–0.93 mm) and somewhat shorter (1.79–2.1 mm). They are thus about half the width of the dorsal ones, but, in each case, two narrow ventral components, slightly subequal in size and shape (Fig. 2E), are sutured to form a single rectangular element of similar size to a dorsal osteoderm. The dorsal osteoderms on the tail are consistent in morphology with those on the body, whereas the ventral osteoderms on the tail are different from those on the trunk, but are similar to the dorsal osteoderms.

**IVPP V 23897 and IVPP V 23898**

Two small blocks were collected from a single pit at Bayan Mandahu in 2012. Both show the same fine sandstone matrix as IVPP V 10080. One block, IVPP V 23898 bears ventral osteoderms like those on the ventral surface of IVPP V 10080 (i.e. long and narrow), as well as a complete right humerus. The second block, IVPP V 23897 bears dorsal osteoderms identical to those on the dorsal surface of IVPP V 10080, in association with a lizard skull, preserved mainly in dorsal view. The osteoderms are preserved just above the left squamosal and quadrate and by the left side of the parietal. Although the bones on the two small blocks are of comparable size, we cannot be fully certain that these blocks represent parts of a single individual.

*IVPP V 23897*. The new skull (Figs. 3, 5) seems to be depressed (contra the description in Gao et Norell, 2000 “laterally compressed”) probably due to preservational distortion. Without further preparation, only the preserved skull roof, postorbital, and the lateral sides of the mandibles are exposed, as well as some dorsal osteoderms identical to those on the dorsum of IVPP V 10080 and in association with the posterior end of a lizard skull. However the µCT scans allow a more complete reconstruction and description. Most of the bones, except the mandibular elements, are slightly displaced from each other.

The parietal (Figs. 3A,B; 5A,C,D) is incomplete, missing its anteriormost part. It has a relatively narrow table that is constricted at the midpoint of the bone as preserved (i.e. posterior to the midpoint of the parietal table itself). The crests separating the skull table from the lateral flanges are very weak. The lateral flanges are extensive and are oriented at a relatively shallow angle to the parietal table so that their surfaces are as much dorsal as

297 lateral. These flanges extend posteriorly and slightly laterally into supratemporal processes
298 with no change in the orientation of their surfaces, thus leaving a large continuous surface of
299 origin for the adductor muscles. The posterior margin of the parietal is roughly U-shaped
300 between the supratemporal processes, and there is no distinct flange or shelf present along
301 the posterior nuchal margin. A small parietal foramen perforates the skull table close to the
302 anterior edge of the preserved parietal (Gao and Norell, 2000, described the parietal foramen
303 as being located slightly anterior to the centre of the table), and there is no trace of
304 sculpturing. This suggests that the overlying dorsal osteoderms and skin were not closely
305 attached to the skull bones. The parietal table as a whole is thickened in the mid-section, but
306 the anterior region and the bases of the supratemporal processes are slightly concave
307 ventrally. The pit for the processus ascendens of the supraoccipital is visible in dorsal view as
308 a notch. It invades the ventral surface of the parietal table for the posterior one quarter of its
309 length, extending deeply due to the thickening of the parietal table. Each supratemporal
310 process projects posterolaterally to a tapered tip, and there is an acute angle between the two
311 processes (less than 90˚). In transverse section, the supratemporal process is laminar, rather
312 than triangular, in shape. A crest divides the dorsal surface of the process into lateral and
313 much narrower medial parts.
314 A small, slender rod-like bone fragment is preserved on the right side of the
315 specimen, and is part of the postorbital ramus of the jugal (Figs. 3A,C; 5A,B,C,D). Although
316 we cannot confirm that the jugal met the postorbital (or postfrontal) in this specimen, the jugal
317 is known to have formed a complete postorbital bar in one of the Mongolian specimens
318 referred to *Parmeosaurus* (IGM 3/139) (Gao and Norell, 2000; The deep scaly project, 2009).
319 On the left side of the parietal, the supratemporal arch is complete with an articulated
320 postorbital and squamosal (Fig. 5A,D), both of which are laminar rather than rod-like. The
321 postorbital bears an anteroventral process that probably met the jugal, and therefore the bone
322 is slightly wider anteriorly in dorsal view. The resolution of the µCT images precludes
323 identification of a facet with certainty. Medially, the postorbital does have a facet for the
324 postfrontal. The postorbital tapers posteriorly, and articulates medially with the squamosal
325 close to its posterior end. The squamosal is a slender bone with a pointed anterior tip, but it
326 widens posteriorly before curving posteroventrally and ending in a pointed tip (probably fitting

into the squamosal notch of the quadrate). The posteromedial surface of the squamosal bears a facet for the supratemporal (Fig. 5A,D). This bone is small and laminar. Its anterior part appears triangular in lateral view, but the bone widens in its mid-section and the ventral edge folds medially to wrap partially under the ventral margin of the parietal supratemporal process. The supratemporal narrows again posteriorly and forms a weak notch that articulates with the cephalic condyle of the quadrate.

The quadrate (Figs. 3A,C; 5A,B,C,D) is stout, with a slender central pillar that is straight in the lower half and curves dorsally. The dorsal and lateral margins, thickened slightly to form a tympanic crest, fold posteriorly to create a deep conch together with the central pillar. The medial lamina is only slightly concave, and is expanded ventrally, with a distinct pterygoid lappet. The medial lamina narrows dorsally and lacks a dorsal border. The dorsal cephalic condyle is small and ovoid, and there seems to be a notch between the condyle and the tympanic crest. The ventral mandibular condyle is mediolaterally elongate, with a very weak groove dividing the condyle into lateral and medial parts. The lateral part is slightly wider anteroposteriorly than the medial one, although it is also slightly smaller in size. Dorsal to the mandibular condyle and on the ventral part of the central pillar, there are two foramina, a small one on the posterior surface (possibly vascular), and a large one on the anterior surface that might have been the exit for the chorda tympani nerve. The two foramina are not connected directly, but open from a cavity within the quadrate.

The palate of IVPP V 23897 preserves only the pterygoids and the right ectopterygoid. The pterygoids (Figs. 5A,B,C,D) are complete except for the tips of the palatine processes. Each is generally Y-shaped, with the ectopterygoid process much shorter than the palatine process. Between the two processes, there is a broad lamina whose anterolateral border contributes the medial and posterior margins of the suborbital fenestra. Two rows of prominent teeth are closely aligned along the medial border of the relatively broad palatine process, and this dentate area reaches to the level at which the ectopterygoid process diverges from the palatine process. The ectopterygoid process is vertically positioned. It forms a prominent posterolateral flange of the main pterygoid lamina in ventral view and a small low flange in dorsal view. The flange bears a medial facet for the ectopterygoid. The joint surface for the basipterygoid process of the basisphenoid lies at almost the same level as the

convergence of the palatine and ectopterygoid processes. An anteroventral shelf extends from the rounded neck of the pterygoid, between the triangular anterior part and the quadrate process, to buttress the movement of the basipterygoid process. The posterior quadrate process is deep, laminar, and vertically positioned. The medial surface is concave, and accommodates the pterygoideus muscles. The pointed posterior tip contacts the pterygoid lappet of the quadrate. Dorsally, at the level of the basipterygoid socket, there is a deep fossa columellae which becomes gradually shallower posteriorly, suggesting that the epipterygoid may have been posteriorly inclined. The epipterygoid itself is long and slender. It is expanded dorsally, where it met either the parietal or the prootic.

The right ectopterygoid (Fig. 5A) is not complete and is represented by the posteromedial ramus that articulated with the pterygoid. The bone is curved as a whole. Its pterygoid ramus bifurcates into a vertical ventral process and a horizontal dorsal process that partially encloses an open medial cavity which accommodated the ectopterygoid process of the pterygoid.

The braincase (Figs. 5G,H) is completely preserved, and has been reconstructed from the μCT slice data. However, the resolution of the CT images makes it difficult to determine clearly the border between the bone and matrix, especially when the bones are thin. For this reason, the reconstructed margins of the bone and some fine structures should be treated with caution. The sutures between the elements, as well as the internal structures, could not be reconstructed. Nevertheless, the μCT reconstruction provides a significant amount of information. The presence of processes and foramina have been checked on both sides, as well as on the μCT slices, to ensure they are genuinely present or absent. Where there is uncertainty, we have been conservative and treated the morphology as unknown.

Two small laminar bones, of similar size, are associated with the braincase. One lies medial to the right epipterygoid and anterior to the main body of the braincase; the other is ventral to the left paroccipital process. Each is roughly pentagonal in shape. Their identification remains uncertain. Orbitosphenoids are a possibility but these are usually triradiate or triangular in shape.

The suture between the basisphenoid and basioccipital is not discernible from the μCT images of IVPP V 23897. This would be consistent with the account of Gao and Norell

(2000) who described the basisphenoid and basioccipital as completely fused in the *Parmeosaurus* specimen IGM 3/140. The floor of the braincase is smooth and without any obvious concavity. The basipterygoid processes are robust and expanded at their distal ends, projecting anterolaterally and slightly ventrally. The angle between the two basipterygoid processes is acute (less than 90˚). In the midline, an ossified parasphenoid rostrum is present for a short length. Gao et Norell (2000) wrote that the rostrum in their *Parmeosaurus* material was well ossified and proportionally robust, but based on this description and the figures, we cannot tell whether the rostrum is long and completely ossified, or it is ossified only posteriorly, with the cartilage trabeculae continuing forward unsupported. The dorsum sellae continues dorsally as the crista sellaris and the crest inclines anteriorly, forming a deep anterior hypophysial cavity. The dorsum sellae is pierced by the abducens foramina, of which posterodorsal and anterior openings are connected by a very short canal. On each side of the hypophysial fossa, the internal carotid foramen is located ventral and medial to the abducens foramen, opening from the vidian canal. The anterior opening of vidian canal is positioned at the junction of the basipterygoid process and the basisphenoid main body (dorsal to the parasphenoid), and the posterior opening is located on the lateral side of the basisphenoid, about halfway between the basipterygoid process and the basal tubercle. The ventral surface of the braincase is elongate and widens posteriorly to the level of the basal tubera, at about three quarters of the braincase length. The tubera point ventrolaterally, and the tubercular crest is weakly developed leaving the occipital recess shallow. Posterior to the tubera, the basioccipital narrows abruptly into the neck of the occipital condyle. The articular surface of the condyle is visible in ventral view with a rounded outline. How much the exoccipitals contributed the occipital condyle is unknown. In posterior view, lateral to the foramen magnum and dorsal to the occipital condyle, there is a depression, the medial wall of which is pierced by a large vagus foramen. Two smaller foramina for the hypoglossal nerve (CN12) lie at the level of the dorsal edge of the occipital condyle, with the two foramina aligned anteroposteriorly. The paroccipital process of the opisthotic is moderately long and extends laterally, ending in a slight expansion.

The supraoccipital bears a median crest which is deep anteriorly and becomes shallower posteriorly towards the dorsal border of the foramen magnum. The anterior border

417 of the bone bears an extension that creates a median notch anterior to the medial crest. This
418 suggests there was a cartilaginous process (ascending process of the supraoccipital)
419 continuing forward to the pit in the parietal. The rounded eminence of the posterior
420 semicircular canal is visible on the surface of the supraoccipital, whereas the anterior and
421 lateral semicircular canals are visible on the lateral side of the braincase. Anterolaterally,
422 there is a well-developed crista prootica, sheltering a depression that is pierced by a single
423 facial foramen. The anterior inferior process of the prootic is prominent and, together with the
424 well developed alar process, encloses a deep notch (incisura prootica) for the trigeminal
425 nerve. This notch is divided into two by a supratrigeminal process that extends from the
426 medial surface of the prootic at the approximate level of the lateral semicircular canal. Further
427 posteriorly, the fenestra vestibuli is rounded and slightly larger than the elongated lateral
428 opening of the recessus scalae tympani. Along the lateral margin of lateral semicircular canal
429 and anterior to the supratemporal facet there is a small process that may be an extra point of
430 articulation for the quadrate.
431 On the medial surface of the braincase, the exit foramen for the endolymphatic duct is
432 visible, as well as an acoustic recess for the foramina of the vestibulocochlear nerve (CN8).
433 However, whether there are one or two acoustic foramina is uncertain.
434 Both lower jaws (Figs. 5E,F) are incomplete and neither the dentaries or splenials are
435 preserved, although there are facets for them on the surangular, coronoid and the angular.
436 The posterior end of the dentary was clearly deeply notched with dorsal and ventral rami of
437 equal length. The facet for the splenial on the coronoid shows that a splenial was present and
438 that its posterior termination almost reached the postero-dorsal end of the dentary. The
439 coronoid bone bears anteromedial, posteromedial and dorsal processes, but no labial or
440 posterior process. The anteromedial process is long, and is separated by a deep notch from
441 the posteromedial process that borders the adductor fossa anteriorly. The dorsal coronoid
442 prominence is high, with an oblique and thickened antero-dorsal border, a posterolateral
443 recess, and a vertical posterior margin. The prominence is also rotated slightly medially. A
444 crest runs from the dorsal tip of the eminence to the ventral end of the posteromedial process,
445 dividing the process into anterior and posterior parts. As a result, the posteromedial process
446 is triangular in section. The angular is slender and long, almost reaching the level of the

anterior margin of the articular facet. Anteriorly for a short distance, it is exposed only on the medial view of the mandible. In its midsection, it is visible in both medial and lateral views (on the ventral border of the mandible), and then only in lateral view posterior to the coronoid bone. The surangular and articular seem to be fused. The two enclose a large adductor fossa, with a small anterior contribution from the coronoid bone. The surangular suspends the dentary and the coronoid anteriorly. Posteriorly the dorsal border of the surangular thickens gradually and forms a triangular platform in front of the articular facet. Laterally, the surangular is pierced by a large anterior surangular foramina at the level of the highest point of the mandible, and a small posterior surangular foramina at the level of the posterior end of the angular. The prearticular process is long, extending anterior to the posterior end of the dentary. There is no angular process. The articular surface is roughly rectangular in shape, longer than wide, and wider medially than laterally. It is orientated with a posteromedial inclination. A very weak ridge separates the surface into medial and lateral parts. The retroarticular process is strongly developed. It is broad, and expanded posteriorly, with a triangular lamina that faces almost medially. The main body is directed posteriorly and is concave dorsally.

A few cranial osteoderms are preserved lateral to the right supratemporal process of the parietal. They are similar to the dorsal body osteoderms of IVPP V 10080 in size and shape. The most completely preserved one is 1.76 wide and 2.69 long (falling within the range of variation of the body osteoderms on IVPP V 10080). Like the dorsal osteoderms, the cranial ones are imbricate anteroposteriorly, with the elevated anterior one-third forming the gliding surface, and they suture laterally.

*IVPP V 23898*. The second small block has little exposed other than osteoderms and a complete right humerus. As noted above, the osteoderms are about half the width of those on the dorsum of the skull block, but these are almost certainly ventral osteoderms. The humerus is of a size that would be consistent with the animal on the skull block. The proximal humeral head is partly obscured by the overlying osteoderms, but appears to have a well-developed deltopectoral crest. The shaft is long and quite slender. The distal head is similar in width to the proximal head, and lies in roughly the same plane. The distal end has a very small

ectepicondyle (but there is no trace of a foramen), a protuberant radial condyle, a smaller rounded ulnar condyle, and a large imperforate entepicondyle. Proximal to the condyles, there is a deep fossa.

**Phylogenetic analysis**

Gao and Norell (2000) tentatively attributed *Parmeosaurus* to the Scincoidea. Most subsequent phylogenetic analyses (Gauthier et al., 2012; Reeder et al., 2015; Pyron, 2017) have supported this attribution, placing *Parmeosaurus* on the scincoid stem. An exception was the analysis of Conrad (2008) which placed *Parmeosaurus* as the sister taxon of Autarchoglossa (sensu Estes et al., 1988).

We first ran an analysis to test whether the Bayan Mandahu material could be grouped together with the Mongolian *Parmeosaurus scutatus*. The original codings in Gauthier et al. (2012), based on the specimens described by Gao and Norell (2000), were used with some revisions (see Table1), and we coded the new material as a second *Parmeosaurus*. The analysis was conducted in TNT version 1.5 (Goloboff and Catalano, 2016), with *Gephyrosaurus* as the outgroup, the full range of taxa coded by Gauthier et al. (2012), and with 128 of the characters ordered (as Gauthier et al., 2012 described). Wagner trees were first obtained, followed by a “New Technology Search: (Sect. Search, Ratchet, and Tree fusing) with the options “Random addition sequences: 1000 number of addseqs”, “20 total number of iterations” for Ratchet, and all the other options as default. One TBR was conducted at the end to search for additional most parsimonious trees. The strict consensus tree of the 192 most parsimonious trees placed the new material and the Mongolian *Parmeosaurus* as sister taxa, which is consistent with the reference of new Bayan Mandahu material to *Parmeosaurus* (see Discussion below).

Following from the results of the first analysis, we combined the data from the Mongolian and Bayan Mandahu specimens and ran a second analysis, using the same parameters as the first. A strict consensus tree of the 96 most parsimonious trees (Fig. 6) places *Parmeosaurus* on the stem of Scincoidea, one node below the Jurassic-Cretaceous genus *Paramacellodus*. This is the same as the maximum parsimony strict consensus tree in Gauthier et al. (2012) (in Reeder et al., 2015 and Pyron, 2017, *Parmeosaurus* is also grouped with *Paramacellodus*).

Note that although Figure 6 shows only the scincoid part of the strict consensus tree, the full range of squamate taxa coded by Gauthier et al. (2012) was run in the analysis (see supplementary figure).

**Discussion**

a) *Attribution of IVPP V 10080*

Gao and Hou (1996) attributed IVPP V 10080 to *Bainguis* based on its rectangular osteoderms and on a small suite of features which they interpreted as anguid synapomorphies, on the premise that *Bainguis* was an anguid. However, of the features they listed most occur more widely within squamates and one is of questionable interpretation:

i) presence of ventral body osteoderms – also occurs in scincoids (e.g. scincids, many cordyliforms), the Jurassic-Cretaceous paramacellodids, and some geckos (Paluh et al. 2017).

ii) rectangular osteoderms that enclose body and tail – also occurs in some scincoids and paramacellodids.

iii) osteoderms that deeply imbricate anteroposteriorly and moderately imbricate laterally. This osteoderm morphology also occurs in paramacellodids and in *Parmeosaurus* (Gao and Norell, 2000).

iv) a relatively long pubis with an elongated and anteriorly directed symphysial process – a derived squamate character but not unique to anguids.

v) the presence of a lateral body fold. This feature is found in some but not all living anguids. However, we could not confirm its presence in IVPP V 10080. There is a lateral cleft but we consider it to be a preservational artefact.

There is therefore no unequivocal support for an anguimorph attribution for IVPP V 10080. However, this alone would not rule out its attribution to *Bainguis*, as the phylogenetic position of that taxon is currently equivocal. Although Borsuk-Białynicka (1984) interpreted *Bainguis* as a stem-anguimorph (‘pre-anguimorph grade’) on the basis of the dentition and a small suite of skull characters, she recognised that none of these characters constituted an unambiguous anguimorph synapomorphy. Moreover, she noted that many of the characteristics of *Bainguis*

could, equally, be used to support attribution to ‘scincomorphs’ or even a position on the stem of Autarchoglossa (sensu Estes et al., 1988). This ambiguity has been reflected in the results of subsequent cladistic analyses. Gao and Norell (1998), reviewing anguimorph relationships, classified *Bainguis* within anguine anguimorphs, although they were unable to score the genus for many of the relevant characters. More importantly, they designated Iguania, Gekkota, and Scincomorpha as outgroups, thereby automatically grouping *Bainguis* with anguimorphs rather than testing its attribution to that clade. The only large morphological data matrix that included *Bainguis* was that of Conrad (2008). His analysis placed *Bainguis* with lacertoids rather than anguimorphs. Conrad et al. (2011) omitted *Bainguis*, as did Gauthier et al. (2012) and Reeder et al. (2015). Pyron (2017) incorporated the Conrad matrix into a calibrated combined data analysis which placed *Bainguis* within scincoids, on the stem of xantusiids.

Whether *Bainguis* had duplex ventral osteoderms is currently unknown, but the presence of these structures in IVPP V 10080 provides an unambiguous synapomorphy with Scincoidea. This, in turn, suggested a relationship with *Parmeosaurus*.

Gao and Norell (2000) attributed *Parmeosaurus* to Scincoidea based on two main characters: 'fronto-maxillary contact'; and 'enlarged coronoid process of dentary overlaps lateral process of coronoid'. They observed that the ventral osteoderms of *Parmeosaurus* were only half the size of the dorsal ones, but did not discuss the potential significance of this observation. Gauthier et al. (2012), however, suggested that the narrower ventral osteoderms might represent components of compound osteoderms, a conclusion we reached separately in IVPP V 10080. Thus IVPP V 10080 and *Parmeosaurus* appear to share the possession of similar duplex ventral osteoderms. There are further similarities in the general morphology of the vertebral column and limbs. The anterior caudal vertebrae of both the *Parmeosaurus* holotype and IVPP V 10080 have caudal ribs, although there is no published information on the length of those ribs in *Parmeosaurus*, and in both specimens the caudals have an autotomy septum lying behind the caudal rib. Based on the scale bar in Gao and Norell's (2000) figure 24, the femur of the *Parmeosaurus* holotype is of similar length to that of IVPP V 10080 (~20.5 mm), suggesting that these lizards were also of equivalent size and proportions. There is thus more evidence linking IVPP V 10080 to *Parmeosaurus* than to *Bainguis*.

b) *Attribution of IVPP V 23897 and V 23898*

The two small blocks provide an additional link between IVPP V 10080 and *Parmeosaurus*. As in both IVPP V 10080 and the Mongolian *Parmeosaurus* specimens, the dorsal osteoderms (IVPP V 23897) are twice the size of the ventral ones (on IVPP V 23898), suggesting the latter form parts of compound osteoderms. The humerus on the IVPP V 23898 block resembles that revealed by µCT scans of IVPP V 10080. Moreover, the mandibles of IVPP V 23897 closely match the description of those of the Mongolian *Parmeosaurus* with respect to the shape of the coronoid bone, the angular (narrow anteriorly but expanding posteriorly to form roughly half the jaw depth), retroarticular process (short and wide with a medial deflection and medial tubercle), and the shape of posterior extremity of the dentary (single surangular notch). The parietal (on IVPP V 23897) also matches that of Mongolian *Parmeosaurus* in having large sloping lateral margins for the attachment of adductor muscles. The quadrate on IVPP V 23897, like that in IGM 3/139, has a large lateral conch. In the posterior palate, the pterygoid bears a double row of teeth, as described for Mongolian *Parmeosaurus*, and the braincase is also closely similar. No difference is observed between IVPP V 23897, IVPP V 23898 and the reported Mongolian *Parmeosaurus* specimens. There thus seems little reason to doubt that the new specimens can also be attributed to *Parmeosaurus.* This attribution (of IVPP V 10080, V 23897, V 23898) to *Parmeosaurus* is also supported by the phylogenetic analysis.

c) *The relationship between* Bainguis *and* Parmeosaurus

Although the original descriptions of *Bainguis* and *Parmeosaurus* place them into different major squamate clades, the equivocal placement of *Bainguis* in recent analyses (Conrad, 2008; Pyron, 2017) raises new questions with respect to their relationship. As described and imaged, *Bainguis* and *Parmeosaurus* share many cranial features including: a rather narrow skull; cranial osteoderms; a series of supraorbitals along the frontal margins; well-developed subolfactory processes on the paired frontals; a maxilla that is triangular in lateral view; adductor muscles arising from lateral edges of the parietal; a jugal meeting the lacrimal anteriorly; a jugal with no posterior spur and a relatively slender postorbital process that forms

most of postorbital border; a separate postfrontal and postorbital, with the postorbital making little orbital contribution but having a long posterior process; and a splenial that is anteriorly long and posteriorly short. In *Bainguis*, the parasphenoid is said to be posteriorly extended to cover most of basioccipital ventrally (Borsuk-Białynicka, 1984). Gao and Norell (2000) were unable to discern a suture between the basisphenoid and basioccipital in *Parmeosaurus*, a condition that could result from a posteriorly extended parasphenoid. However, there are also some points of difference in the descriptions, most notably:

i) *Bainguis* was described (Borsuk-Białynicka, 1984, p.25) as having 'low, broad, conical' maxillary teeth and mandibular teeth that were longer and more slender, but too badly damaged for detailed comparison. In contrast, *Parmeosaurus* is said to have only 4–5 conical teeth anteriorly, followed by bicuspid, then robust tricuspid teeth (Gao and Norell, 2000). Although specimens of *Parmeosaurus* are somewhat larger than the holotype of *Bainguis*, the size difference would not account for the difference in the dentition if adults or even sub-adults are being compared. However, the figured lower jaw of *Bainguis* (Borsuk-Białynicka, 1984; fig. 6) seems to be based on that of a much smaller juvenile skull (MgR-II/90, as figured in Borsuk-Białynicka, 1984: plate 3.3a) that was referred to *Bainguis* mainly on the basis of proportional similarities. Re-examination of the *Bainguis* specimens by one of us (LD) found too few points of comparison to confirm the attribution of the juvenile skull to *Bainguis*. For the present, therefore, discussion of *Bainguis* should be limited to the holotype in which the lower jaw has around 12 tooth positions. As preserved, the teeth are relatively homodont and conical, but the tips are eroded. This makes comparison with *Parmeosaurus* difficult.

ii) As figured (Borsuk-Białynicka, 1984; fig.6), the lower jaw of *Bainguis* is more gracile than that of *Parmeosaurus*, with a much longer retroarticular process. However, if this reconstruction is based on the referred juvenile MgR-II/90, then it may not be comparable for the reason outlined above. The jaw of the *Bainguis* holotype is also relatively gracile but appears to have a short (or incomplete) retroarticular process (Borsuk-Białynicka, 1984; plate 3: 2a, b).

iii) *Bainguis* was described as having no alar process on the prootic, whereas *Parmeosaurus* has one. Our re-examination of *Bainguis* confirms this distinction.

iv) *Bainguis* was figured as having the nasal meeting the prefrontal to exclude the frontal from the maxilla, whereas *Parmeosaurus* was described as having the frontal meeting the maxilla. Our re-examination of the *Bainguis* holotype confirms this distinction.

v) The original description of *Bainguis* noted the presence of postcranial material but this was not described and the only elements figured were a group of attributed vertebrae (Borsuk-Białynicka, 1984: plate 2:1e). The postcranial specimens were referred to *Bainguis* on the basis of associated rectangular osteoderms, but re-examination of this material by one of us (LD) suggests that the postcranial material in the ZPAL collections is more likely to represent *Parmeosaurus*. The morphology of the hind limb, size and shape of the osteoderms (larger than those on the neck of the *Bainguis* holotype), and the pattern of autotomy septa in the tail all provide a better match with the figured holotype of *Parmeosaurus* (Gao and Norell, 2000).

## Conclusions

Re-assessment of IVPP V 10080 suggests it is a stem-scincoid, rather than an anguimorph as originally proposed (Gao and Hou, 1996). It most closely resembles *Parmeosaurus* (Gao and Norell, 2000) as currently diagnosed, and phylogenetic analysis supports its attribution to that taxon. IVPP V 23897 and V 23898 are also attributable to *Parmeosaurus* based on the similarity of the parietal, palate and braincase, as well as the postdentary mandible. The lizard faunal list for Bayan Mandahu must therefore be revised. *Bainguis* and *Parmeosaurus* appear to be distinct genera, but postcranial material originally referred to the former is probably attributable to the latter, and the status of a juvenile skull referred to *Bainguis* is also uncertain. Determining whether *Bainguis,* as represented by the holotype skull*,* is an anguimorph or a scincoid related to *Parmeosaurus* will require the recovery of more complete adult material.

## Acknowledgements

The authors are grateful to Tao Yu and Lishi Xiang (IVPP, CAS) who recovered and prepared respectively IVPP V 23897 and IVPP V 23898 from Bayan Mandahu; and to Yemao Hou (IVPP, CAS) for help with the CT scanning. The research was supported by the fund from the State Key Laboratory of Palaeobiology and Stratigraphy (Nanjing Institute of Geology and

Palaeontology, Chinese Academy of Sciences, Nanjing) (No. 163106), and the National Natural Science Foundation of China (Grant No. 41688109). The CAS President's International Fellowship Initiative awarded to SEE in 2016 supported her visit to IVPP, CAS, during which this work was undertaken. An inter-Academies exchange grant from CAS funded LD's stay at the Institute of Paleobiology, Polish Academy of Sciences, Warsaw, Poland, in 2017. The collection and preparation of the IVPP V 23897 and IVPP V 23898 were supported by the National Natural Science Foundation of China (Grant No.41120124002). We thank Prof. Magdalena Borsuk-Białynicka and Ms. Jolanta Kobylińska (Institute of Paleobiology, Polish Academy of Sciences) for access to the attributed material of *Bainguis* and for their help and hospitality during LD's visit. Our thanks also go to the reviewers, Juan D. Daza and Randall L. Nydam, and to the editors for their helpful comments on an earlier version of the manuscript.

**References**

1. Borsuk-Białynicka, M., 1984. Anguimorphans and related lizards from the Late Cretaceous of the Gobi Desert, Mongolia. Palaeontologica Polonica 46: 5–105.
2. Borsuk-Białynicka, M., 2007. Evolution of the iliosacral joint in diapsid phylogeny. Neues Jahrbuch für Geologie und Paläontologie - Abhandlungen 249: 297–311.
3. Brinkman D., Peng J.H., 1996. A new species of *Zangerlia* (Testudines: Nanhsiungchelyidae) from the Upper Cretaceous redbeds at Bayan Mandahu, Inner Mongolia, and the relationships of the genus. Canadian Journal of Earth Sciences 33: 526–540.
4. Conrad, J.L., 2008. Phylogeny and systematic of Squamata (Reptilia) based on morphology. Bulletin of the American Museum of Natural History 310: 1–182.
5. Conrad, J.L., Ast, J.C., Montari, S., Norell, M.A., 2011. A combined evidence phylogenetic analysis of Anguimorpha (Reptilia, Squamata). Cladistics 27: 230–277.
6. Dong, Z.M., Currie, P.J., 1996. On the discovery of an oviraptorid skeleton on a nest of eggs at Bayan Mandahu, Inner Mongolia, People's Republic of China. Canadian Journal of Earth Sciences 33: 631–636.

685 **7.** Eberth, D.A., 1993. Depositional environments and facies transitions of dinosaur-bearing
686 Upper Cretaceous redbeds at Bayan Mandahu (Inner Mongolia, People's Republic of
687 China). Canadian Journal of Earth Sciences 30: 2196–2213.
688 8. Estes, R., de Queiroz, K., Gauthier, J., 1988. Phylogenetic relationships within
689 Squamata. In: Estes, R., Pregill, G. eds, Phylogenetic relationships of the lizard families
690 — Essays Commemorating Charles L. Camp. Stanford University Press, Stanford,
691 California, 119–281.
692 9. Gao, K.Q., Hou, L.H., 1995. Iguanians from the Upper Cretaceous Djadochta Formation,
693 Gobi Desert, China. Journal of Vertebrate Paleontology 15: 57–78.
694 10. Gao, K.Q., Hou, L.H., 1996. Systematics and taxonomic diversity of squamates from the
695 Upper Cretaceous Djadochta Formation, Bayan Mandahu, Gobi Desert, People's
696 Republic of China. Canadian Journal of Earth Sciences 33: 578–598.
697 11. Gao, K.Q., Norell, M., 1998. Taxonomic revision of *Carusia* (Reptilia: Squamata) from the
698 Late Cretaceous of the Gobi Desert and phylogenetic relationships of anguimorphan
699 lizards. American Museum Novitates 3230: 1–51.
700 12. Gao, K.Q., Norell, M., 2000. Taxonomic composition and systematic of the Late
701 Cretaceous lizard assemblages from Ukhaa Tolgod and adjacent localities, Mongolian
702 Gobi Desert. Bulletin of the American Museum of Natural History 249: 1–118.
703 13. Gauthier, J.A., Kearney, M., Maisano, J.A., Rieppel, O., Behlke, A., 2012. Assembling
704 the squamate tree of life: perspectives from the phenotype and the fossil record. Bulletin
705 of the Peabody Museum of Natural History 53: 3–308.
706 14. Goloboff, P. A., Catalano, S. A., 2016. TNT version 1.5, including a full implementation of
707 phylogenetic morphometrics. Cladistics 32: 221–238.
708 15. Jerzykiewicz, T., Currie, P.J., Eberth, D.A., Johnston, P.A., Koster, E.H., Zheng, J.J.,
709 1993. Djadokhta Formation correlative strata in Chinese Inner Mongolia: an overview of
710 the stratigraphy, sedimentary geology, and paleontology and comparisons with the type
711 locality in the pre-Altai Gobi. Canadian Journal of Earth Sciences 30: 2180–2190.
712 16. Ladevèze, S., de Muizon, C., Colbert, M., Smith, T., 2010. 3D computational imaging of
713 the petrosal of a new multituberculate mammal from the Late Cretaceous of China and
714 its paleobiologic inferences. Comptes Rendus Palevol 9: 319–330.

715 17. Makovicky, P.J., 2008. Telling time from fossils: a phylogeny-based approach to
716 chronological ordering of paleobiotas. Cladistics 24: 350–371.
717 18. Meng, J., 2014. Mesozoic mammals of China: implications for phylogeny and early
718 evolution of mammals. National Science Review 1: 521–542.
719 19. Oppel, M., 1811. Die Ordnungen, Familien und Gattungen der Reptilien als Prodom einer
720 Naturgeschichte Derselben. Joseph Lindauer, München xii-86.
721 20. Paluh, D. J., Griffing, A. H., Bauer, A. M., 2017. Sheddable armour: identification of
722 osteoderms in the integument of (Gekkota). African Journal of Herpetology 66: 12–24.
723 21. Pittman, M., Xu, X., Stiegler, J.B., 2015. The taxonomy of a new parvicursorine
724 alvarezsauroid specimen IVPP V20341 (Dinosauria: Theropoda) from the Upper
725 Cretaceous Wulansuhai Formation of Bayan Mandahu, Inner Mongolia, China. PeerJ 3,
726 e986.
727 22. Pyron, R.A., 2017. Novel approaches for phylogenetic inference from morphological data
728 and total-evidence dating in squamate reptiles (lizards, snakes, and amphisbaenians).
729 Systematic Biology 66: 38–56.
730 23. Reeder, T.W., Townsend, T.M., Mulcahy, D.G., Noonan, B.P., Wood Jr., P.L., Sites Jr.,
731 J.W., Wiens, J.J., 2015. Integrated analyses resolve conflicts over squamate reptile
732 phylogeny and reveal unexpected placements for fossil taxa. PLoS ONE 10: e0118199.
733 24. Russell, A.P., Bauer, A.M., 2008. The appendicular locomotor apparatus of Sphenodon
734 and normal-limbed squamates. In: Gans, C., Gaunt, A.S., Adler, K. eds, Biology of the
735 Reptilia, volume 21, Morphology 1. The skull and appendicular apparatus of
736 Lepidosauria. Society for the Study of Amphibians and Reptiles. Ithaca, New York, 1–
737 465.
738 25. Snyder, R.C., 1954. The anatomy and function of the pelvic girdle and hindlimb in lizard
739 locomotion. The American Journal of Anatomy 95: 1–43.
740 26. Tałanda, M., 2016. Cretaceous roots of the amphisbaenian lizards. Zoologica Scripta 45:
741 1–8.
742 27. The Deep Scaly Project, 2009, "*Parmeosaurus scutatus*" (On-line), Digital Morphology.
743 Accessed July 18, 2017 at http://digimorph.org/specimens/Parmeosaurus_scutatus/.

744 28. Wu, X.C., Brinkman, D.B., Russell, A.P., Dong, Z.M., Currie, P.J., Hou, L.H., Cui, G.H.,
745 1993. Oldest known amphisbaenian from the Upper Cretaceous of Chinese Inner
746 Mongolia. Nature 366: 57–59.
747 29. Wu, X.C., Brinkman, D.B., Russell, A.P., 1996. *Sineoamphisbaena hexatabularis*, an
748 amphisbaenian (Diapsida: Squamata) from the Upper Cretaceous redbeds at Bayan
749 Mandahu (Inner Mongolia, People's Republic of China), and comments on the
750 phylogenetic relationships of the Amphisbaenia. Canadian Journal of Earth Sciences 33:
751 541–577.
752 30. Xu, X., Tan, Q.W., Wang, S., Sullivan, C., Hone, D.W.E., Han, F.L., Ma, Q.Y., Tan, L.,
753 Xiao, D., 2013. A new oviraptorid from the Upper Cretaceous of Nei Mongol, China, and
754 its stratigraphic implications. Vertebrata PalAsiatica 51: 85–101.
755 31. You, H.L., Dong, Z.M., 2003. A new protoceratopsid (Dinosauria: Neoceratopsia) from
756 the Late Cretaceous of Inner Mongolia, China. Acta Geologica Sinica (Engl Ed) 77: 299–
757 303.
758

**Table 1 Codings for *Parmeosaurus scutatus*. (A=0 or 1; B=1 or 2)**

| | | | | |
|---|---|---|---|---|
| Gauthier et al. (2012) | | 1000001?00 | 00000?0??0 | 0??0000000 |
| 000??01010 | 000?0?0?30 | 00000?110? | ?001000000 | 0?0?00???0 |
| 0?2?0??100 | ??000?100? | 0110000?0 | 0??301?000 | 0000000100 |
| 00000????? | ?001?00020 | 000???10?? | ?????0??0? | 0?0???1?**0**0 |
| 1**B**00?0???? | ???0?00?11 | ?000???2?? | ?0?0??1??1 | 00?000??01 |
| ?0000????? | ?0??100003 | ?0?1001??? | 0000?000?0 | ?10?2000?0 |
| 00**2**02??0?0 | ?00?12?000 | **1**0????00?0 | 00???????? | 0?0000???? |
| ?001?1?00? | 0?0???0??0 | ??01??0002 | 30?0001**1**00 | 0000300000 |
| 100?101?02 | 0?10?0000**0** | 0000**1**00001 | 0010000033 | 3000000000 |
| 00020?0??? | ?????????? | ?????????? | 0?2?0?1??? | 0??????0?? |
| ???????00? | ?????????? | ?????????0 | ?????0???0 | **0**000??00?**?** |
| ?????????? | ???????0?0 | ????1????? | ?????????1 | 0**0**1020221? |
| 010??????? | ?????????? | ?????????? | | |
| New codings based on all available material | | 1000001?00 | 00000?0??0 | |
| 0??0000000 | 000??01010 | 000?0?0?30 | 00000?110? | ?001000000 |
| 0?0000010? | 0B200?0100 | 0?0003100? | 01100000A0 | 0??301?000 |
| 0000000100 | 00000????? | ?001?00020 | 00010?1000 | 000010000A |
| 0?00001100 | 1B00402??? | ??30?00?11 | ?000???2?? | ?0?0??1??1 |
| 00?000??01 | ?0000????? | ?0??100003 | ?0?1001B?? | 0000?00000 |
| 0020201000 | 010?2000?0 | ?00?121000 | 10?0010000 | 000??????0 |
| 0?0000???? | ?001?1000? | 0000??0000 | ?101??0002 | 30?0001100 |
| 0000300000 | 1001101?02 | 0?10?00000 | 0000100001 | 00B0000033 |
| 3000000000 | 00020?0??? | ?????????? | ???0B0000? | 0?2?0?1A02 |
| 000021?0?? | ???????00? | ????1???02 | 1??0001110 | 1110100??0 |
| 0000??00?? | ?????????? | ???????000 | ????110000 | ???0?????1 |
| 0010202212 | 010??????? | ?????????? | ?????????? | |

We checked the character codings for the Mongolian *Parmeosaurus* from the description in Gao et Norell 2000 and the surface model from The Deep Scaly Project 2009, and revised a small number of these. The revised characters in the Gauthier et al. (2012) matrix are shown in bold.

Figure 1 Map of fossil localities that yield *Bainguis* and *Parmeosaurus* material (indicated by stars). The *Parmeosaurus* material reported by Gao and Norell (2000) is from Ukhaa Tolgod, Mongolia; The new *Parmeosaurus* material here in this paper is from Bayan Mandahu, China; The *Bainguis* material (Borsuk-Białynicka, 1984) is from Bayn Dzak, Mongolia.

Figure 2 *Parmeosaurus scutatus*, referred specimen IVPP V 10080. A, B. postcranial skeleton in dorsal (A) and ventral (B) views; C. pectoral girdle part in ventral view; D. dorsal osteoderms; E. ventral osteoderms. The squares in A and B indicate the area where D and E are from. Scale bars = 5 mm.

Figure 3 *Parmeosaurus scutatus*, referred specimen IVPP V 23897 in dorsal (A), ventral (B), right lateral (C) and left lateral (D) views. Scale bar = 10 mm.

Figure 4 *Parmeosaurus scutatus*, referred specimen IVPP V 10080, 3D rendering of the CT scan data. A, B. postcranial skeleton in dorsal (A) and ventral (B) views; C. right pelvis and hind limb reconstructed on the posterolateral view.

Figure 5 *Parmeosaurus scutatus*, referred specimen IVPP V 23897, 3D rendering of the CT scan data. A, B. the complete specimen in dorsal (A), ventral (B), right lateral (C), left lateral (D) views; E, F. the preserved right lower jaw in lateral (E) and medial (F) views; G, H. the braincase segmented out from the specimen in anterior (G) and lateroventral (H) views; Scale bar = 10 mm; E, F, G, H are not to scale.

Figure 6 The scincoid part of the strict consensus tree showing the position of *Parmeosaurus scutatus*. The analyses adopted Gauthier et al. (2012)'s matrix, revised the coding of *Parmeosaurus,* used the "new technology search" method, and got 96 most parsimonious trees. Bootstrap values above each branch and Bremer values below each branch were obtained in TNT by the embedded bootstrap command and Bremer. run script respectively. The consensus tree failed to resolve the relationship between the large groups, but is stable,

820 as far as the scincoid part is concerned. The complete result of the analysis see

821 supplementary Figure.

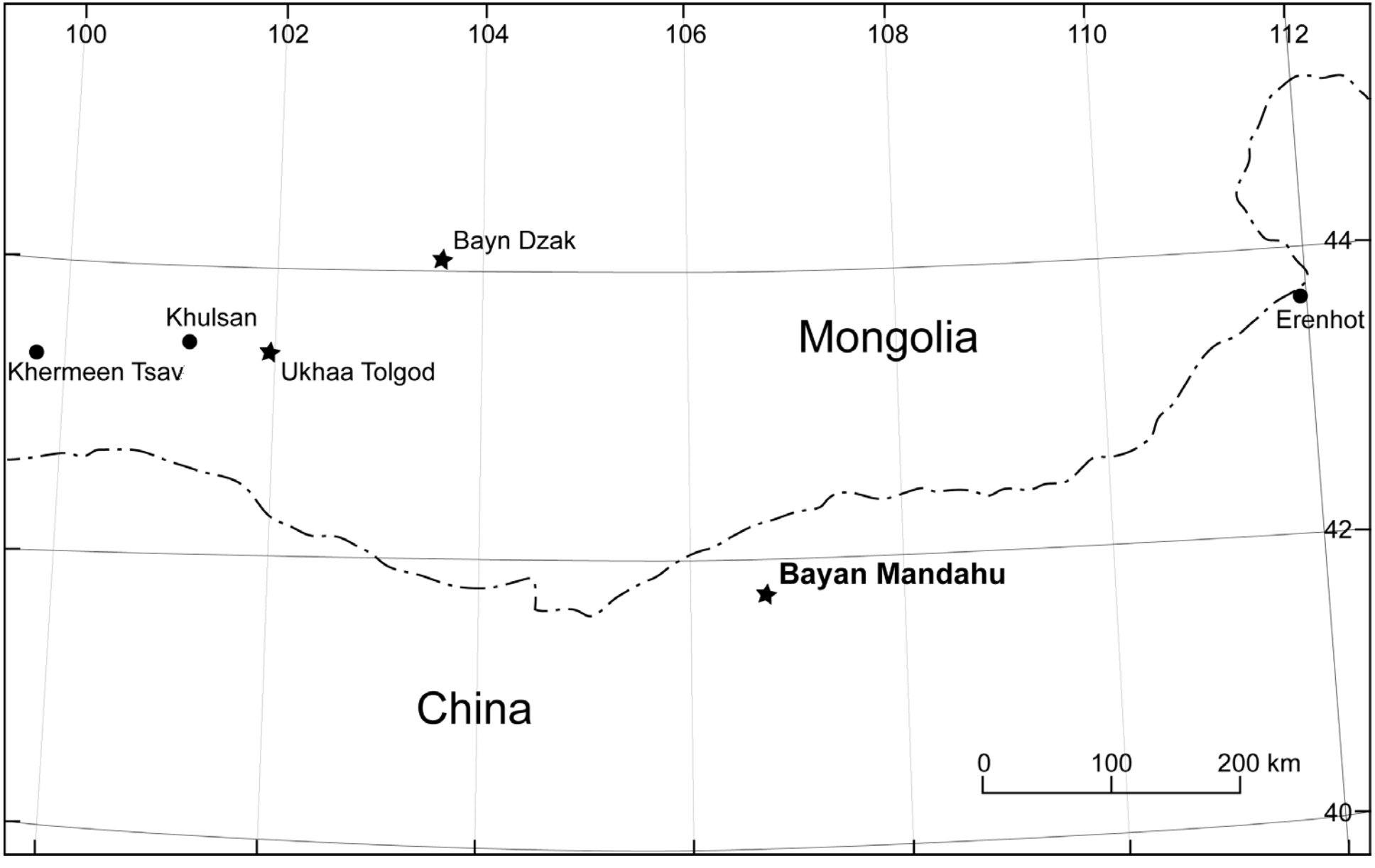
100
102
104
106
108
110
112
44
42
40
Bayn Dzak
Khulsan
Khermeen Tsav
Ukhaa Tolgod
Mongolia
Erenhot
Bayan Mandahu
China
0
100
200 km

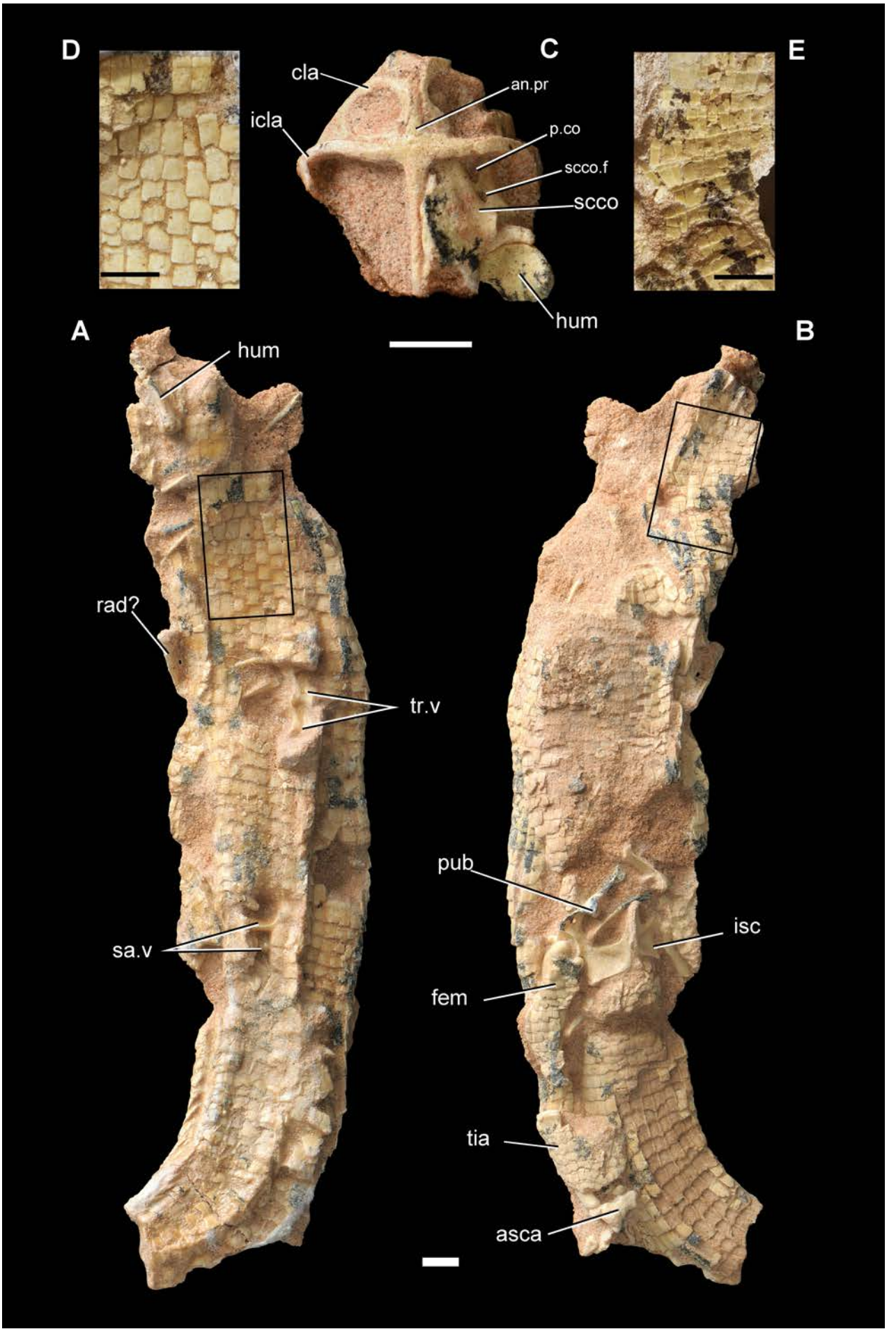
D
C
E
cla
an.pr
icla
p.co
scco.f
scco
hum
A
B
hum
rad?
tr.v
pub
isc
sa.v
fem
tia
asca

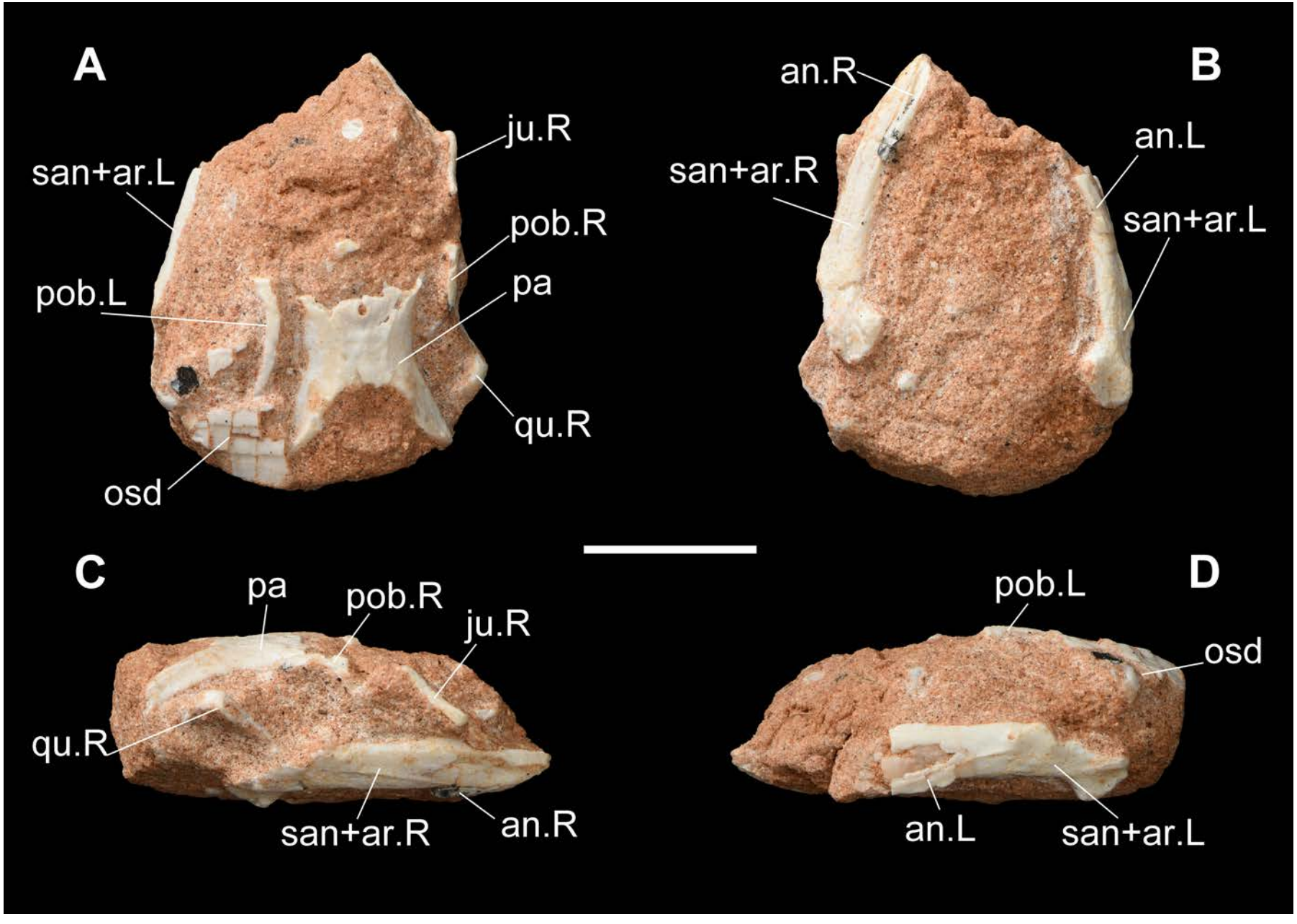
A
ju.R
san+ar.L
pob.R
pob.L
pa
qu.R
osd
B
an.R
an.L
san+ar.R
san+ar.L
C
pa
pob.R
ju.R
qu.R
san+ar.R
an.R
D
pob.L
osd
an.L
san+ar.L

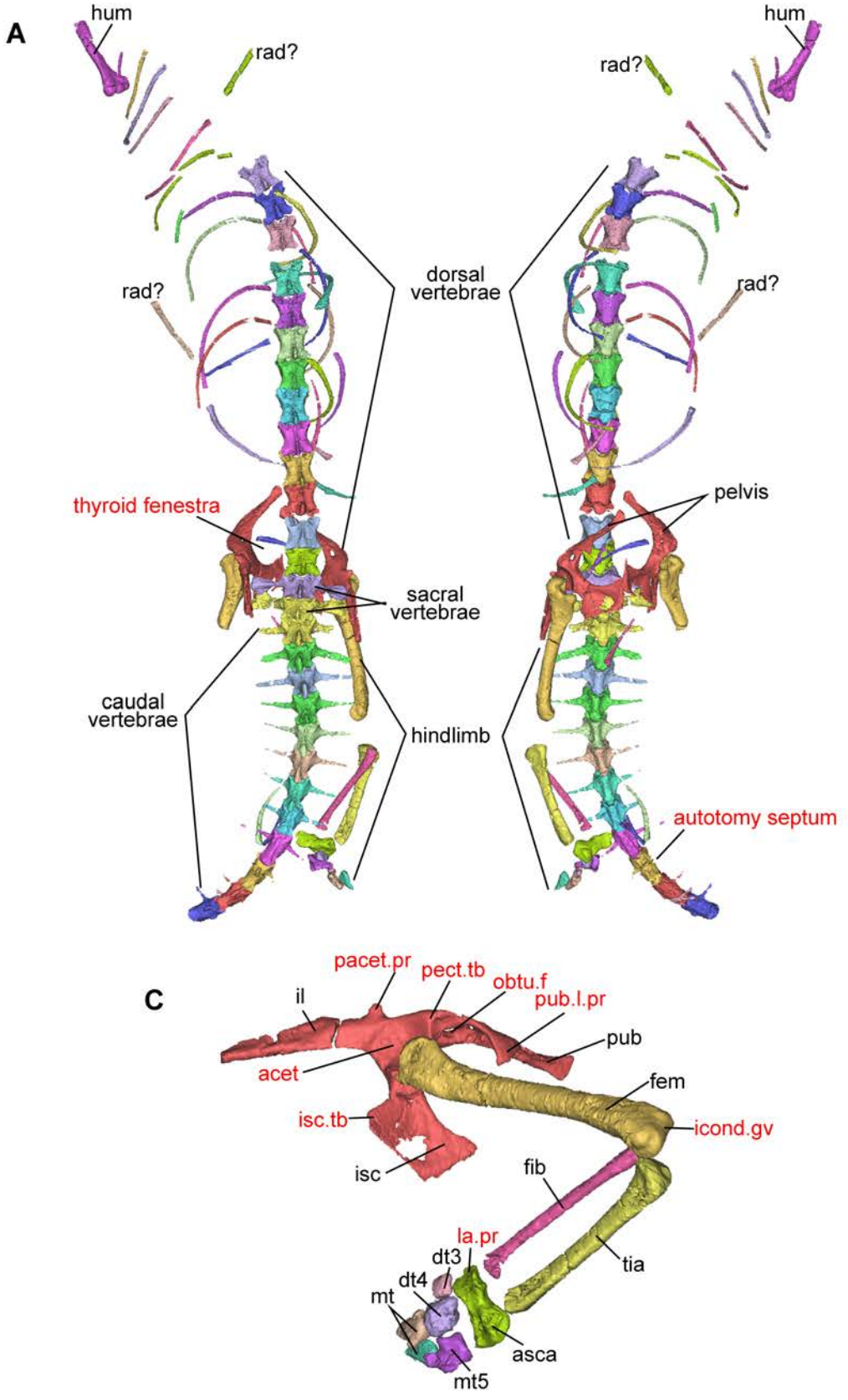
A
hum
rad?
rad?
dorsal vertebrae
thyroid fenestra
sacral vertebrae
caudal vertebrae
hindlimb
B
hum
rad?
rad?
pelvis
autotomy septum
C
pacet.pr
pect.tb
obtu.f
il
pub.l.pr
pub
acet
fem
isc.tb
icond.gv
isc
fib
la.pr
dt3
tia
dt4
mt
asca
mt5

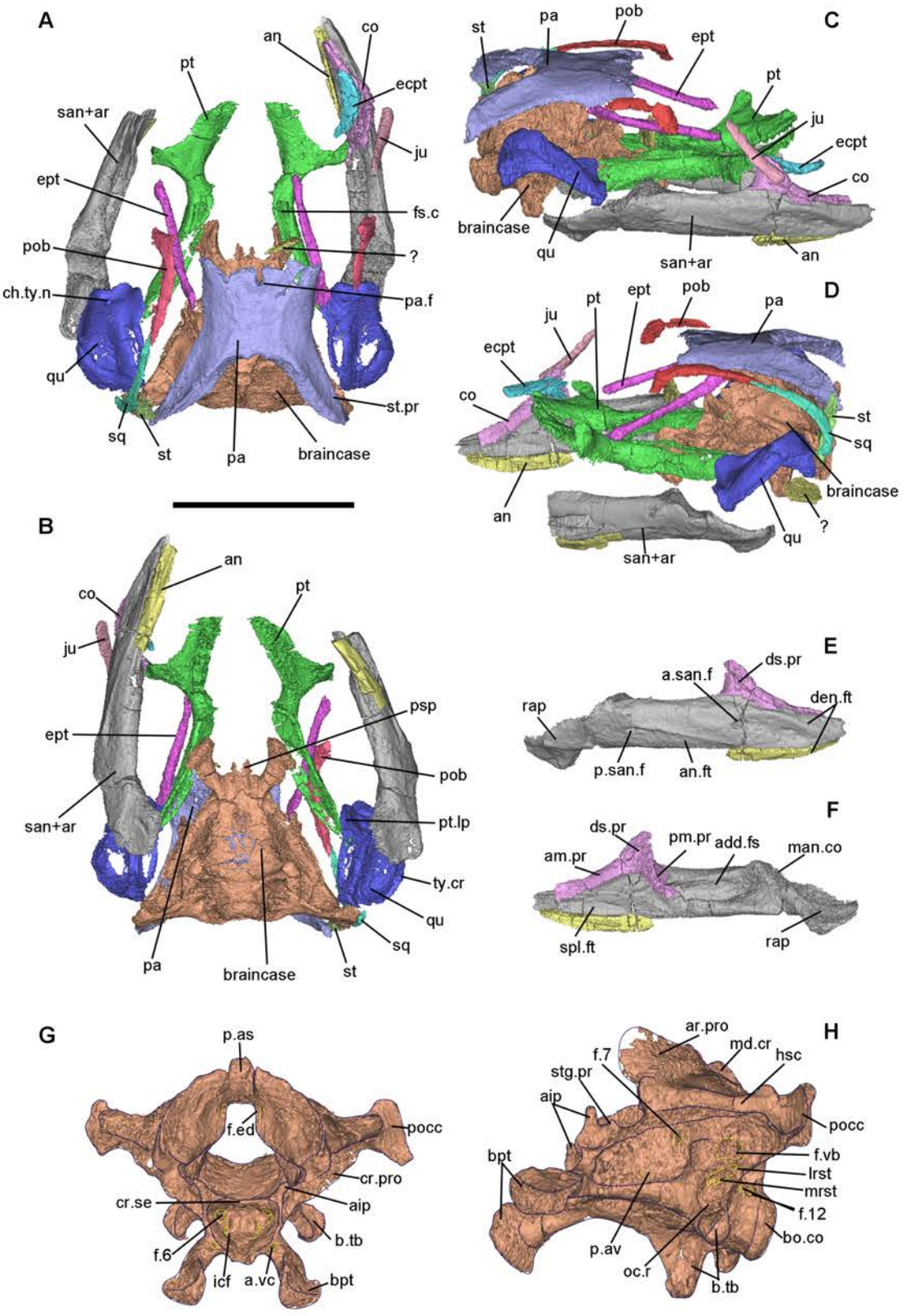
A
an
co
pt
ecpt
san+ar
ju
ept
fs.c
pob
?
ch.ty.n
pa.f
qu
st.pr
sq
st
pa
braincase
B
an
co
pt
ju
psp
ept
pob
san+ar
pt.lp
ty.cr
qu
sq
pa
braincase
st
C
st
pa
pob
ept
pt
ju
ecpt
co
braincase
qu
san+ar
an
D
ju
pt
ept
pob
pa
ecpt
co
st
sq
braincase
an
qu
?
san+ar
E
a.san.f
ds.pr
den.ft
rap
p.san.f
an.ft
F
ds.pr
pm.pr
add.fs
man.co
am.pr
spl.ft
rap
G
p.as
f.ed
pocc
cr.pro
cr.se
aip
b.tb
f.6
icf
a.vc
bpt
H
ar.pro
md.cr
hsc
f.7
stg.pr
aip
pocc
bpt
f.vb
lrst
mrst
f.12
bo.co
p.av
oc.r
b.tb

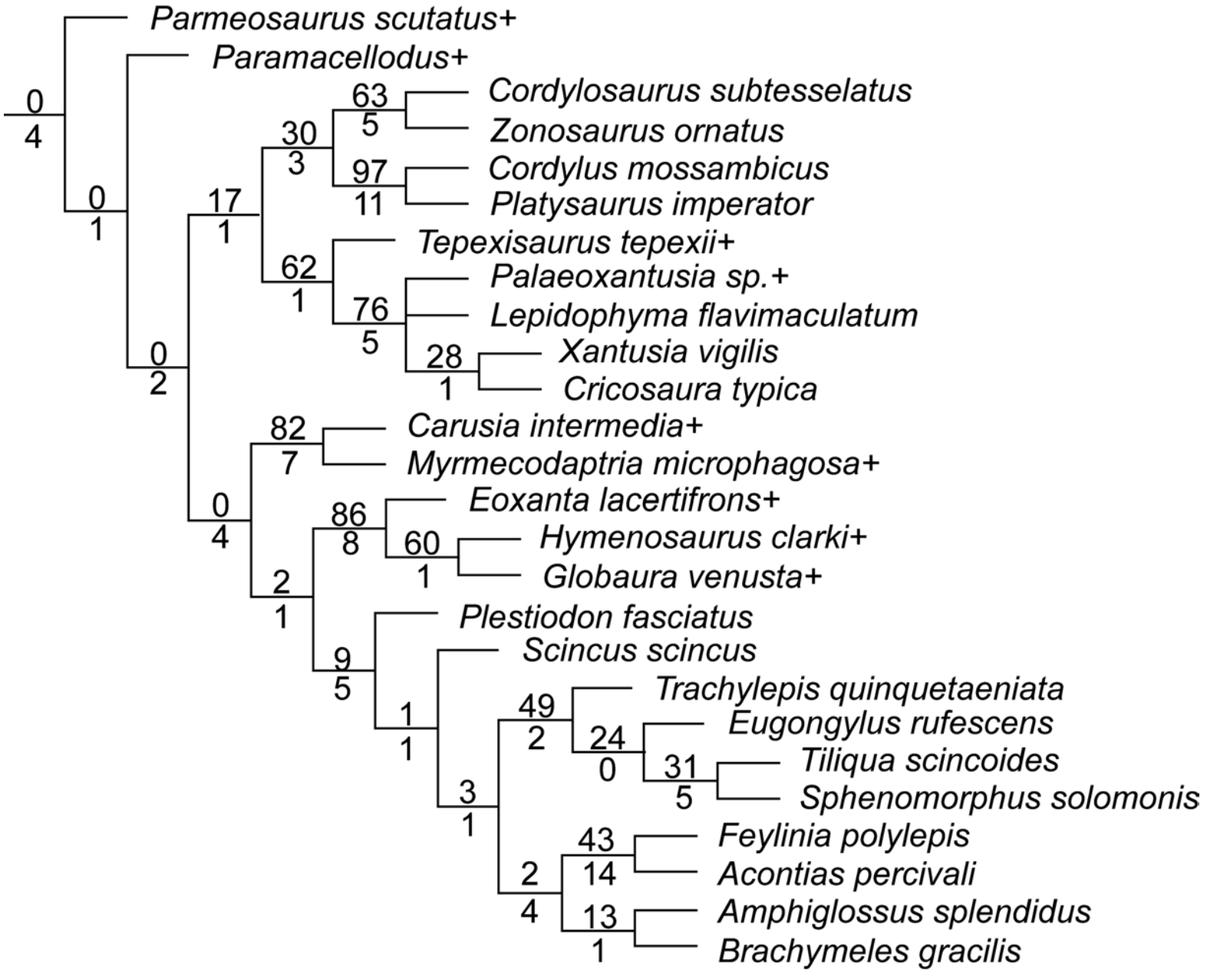
Parmeosaurus scutatus+
Paramacellodus+
Cordylosaurus subtesselatus
Zonosaurus ornatus
Cordylus mossambicus
Platysaurus imperator
Tepexisaurus tepexii+
Palaeoxantusia sp.+
Lepidophyma flavimaculatum
Xantusia vigilis
Cricosaura typica
Carusia intermedia+
Myrmecodaptria microphagosa+
Eoxanta lacertifrons+
Hymenosaurus clarki+
Globaura venusta+
Plestiodon fasciatus
Scincus scincus
Trachylepis quinquetaeniata
Eugongylus rufescens
Tiliqua scincoides
Sphenomorphus solomonis
Feylinia polylepis
Acontias percivali
Amphiglossus splendidus
Brachymeles gracilis
0
4
0
1
63
5
30
3
97
11
17
1
62
1
76
5
28
1
0
2
82
7
0
4
86
8
60
1
2
1
9
5
1
1
3
1
49
2
24
0
31
5
2
4
43
14
13
1